Title

Signaling dynamics distinguish high- and low-priority neutrophil chemoattractant receptors

Journal

Science Signaling, 16(805)

ISSN

1945-0877

Authors

Lundgren, Stefan M

Rocha-Gregg, Briana L

Akdoğan, Emel

et al.

Publication Date

2023-10-03

DOI

10.1126/scisignal.add1845

Peer reviewed

Published in final edited form as:
Sci Signal. 2023 October 03; 16(805): eadd1845. doi:10.1126/scisignal.add1845.

Signaling dynamics distinguish high and low priority neutrophil chemoattractant receptors

Stefan M. Lundgren[1,†], **Briana L. Rocha-Gregg**[1,†], **Emel Akdoğan**[1], **Maya N. Mysore**[1], **Samantha Hayes**[1], **Sean R. Collins**[1,*]

[1]Department of Microbiology and Molecular Genetics, University of California, Davis, Davis, CA 95616, USA.

Abstract

Human neutrophils respond to multiple chemoattractants to guide their migration from the vasculature to sites of infection and injury, where they clear pathogens and amplify inflammation. To properly focus their responses during this complex navigation, neutrophils prioritize pathogen- and injury-derived signals over long-range inflammatory signals, such as the leukotriene LTB4, secreted by host cells. Different chemoattractants can also drive qualitatively different modes of migration even though their receptors couple to the same $G\alpha_i$ family of G proteins. Here, we used live-cell imaging to demonstrate that the responses differed in their signaling dynamics. Low-priority chemoattractants caused transient responses, whereas responses to high-priority chemoattractants were sustained. We observed this difference in both primary neutrophils and differentiated HL-60 cells, for downstream signaling mediated by Ca^{2+}, a major regulator of secretion, and Cdc42, a primary regulator of polarity and cell steering. The rapid attenuation of Cdc42 activation in response to LTB4 depended on the phosphorylation sites Thr^{308} and Ser^{310} in the C-terminal tail of its receptor LTB4R in a manner independent of endocytosis. Mutation of these residues to alanine impaired chemoattractant prioritization, although it did not affect chemoattractant-dependent differences in migration persistence. Our results indicate that distinct temporal regulation of shared signaling pathways distinguishes between receptors and contributes to chemoattractant prioritization.

INTRODUCTION

Neutrophils play central roles in inflammation and defense against microbial pathogens by responding rapidly to chemical signals and migrating to sites of injury or infection

*Corresponding author. srcollins@ucdavis.edu.
†These authors contributed equally to this work.

Author contributions:
Conceptualization: BLRG, SML, SRC
Methodology: SML, BLRG, SH, MNM, EA, SRC
Investigation: SML, BLRG, SH, MNM, EA, SRC
Formal analysis: SML, BLRG, EA, SRC
Software: BLRG, SML, SRC
Funding acquisition: SRC, BLRG
Writing – original draft: SML, BLRG, EA, SRC
Writing – review & editing: SML, BLRG, SH, EA, SRC

Competing interests: The authors declare that they have no competing interests.

(1, 2). Once there, they mount cytotoxic responses including phagocytosis, degranulation, production of reactive oxygen species, and the release of anti-microbial extracellular traps (3). They also amplify inflammation by secreting factors that recruit additional immune cells (4). These activities are critical for effective immune responses, but their dysregulation is a major cause of tissue damage and chronic inflammation in autoimmune and inflammatory diseases (5–7).

Central to both productive and pathological inflammation, neutrophils navigate to target locations through chemotaxis, sensing gradients of chemoattractants with cell surface receptors. These receptors are almost uniformly G-protein coupled receptors (GPCRs) that couple to the $G\alpha_i$ family of G-proteins. Although each of these receptors can drive chemotaxis, the behavioral responses to them are not identical. Different chemoattractants can drive modes of migration that qualitatively differ in the directedness of their migratory paths (8), the gradient sensing strategies used (9), and the prioritization status when cells encounter competing gradients of different ligands (10–12).

Prioritization between chemoattractants enables neutrophils to transition between guidance cues in complex environments where multiple chemoattractants often form overlapping gradients (1). Characteristically, host-secreted molecules such as the chemokine interleukin-8 (IL8) and the signaling lipid leukotriene B4 (LTB4) act as “intermediary” signals, guiding neutrophils out of the vasculature and into the general vicinity of their target. However, these intermediary signals are ignored once neutrophils detect “end-target” signals near their ultimate destination. These injury or pathogen-derived signals, such as complement factor 5a (C5a) and formylated peptides, are prioritized to focus neutrophils’ cytotoxic activities on the appropriate targets.

Differences in migration modes and prioritization status can be recapitulated in vitro, where cellular decisions depend almost entirely on the chemoattractant identities and are largely independent of their relative concentrations (8, 10–12). However, the molecular mechanisms controlling these differences are not fully clear. In the case of prioritization, multiple mechanisms have been proposed, but it remains unclear whether prioritization is achieved through receptor-level regulation or crosstalk between downstream pathways (10–17).

In response to both intermediary and end-target chemoattractants, receptor activation leads to a downstream signaling cascade driven by effectors of both $G\alpha_i$ and $G\beta\gamma$ subunits, including Rac, Cdc42, RhoA, Ca^{2+} signaling, and reorganization of the actin cytoskeleton (Fig. 1A) (18). Cdc42 has been implicated as a primary regulator of cell polarity and cell-steering, making it an intriguing candidate for investigating potential differences in intermediary and end-target signaling inputs (19–21).

Here, we found that the dynamics of signaling responses downstream of end-target and intermediary receptors differed, with end-target receptors generating a more sustained signaling response. We found that rapid attenuation of the response to LTB4 depended on the Thr^{308} and Ser^{310} phosphorylation sites in the C-terminal tail of the receptor LTB4R. Alanine substitution of these two residues resulted in a sustained signaling response similar to that generated by the formyl peptide receptor, and it resulted in impaired prioritization of

formyl peptide over LTB4. However, these mutations did not affect differences in migration persistence between these two chemoattractants. Our experimental results are consistent with theoretical analysis demonstrating that homologous receptor desensitization could determine prioritization status (15). Our results suggest that signal output duration is a distinguishing feature between end-target and intermediary chemoattractant receptors, and that these differences in signaling dynamics contribute to chemoattractant prioritization.

RESULTS

Chemoattractant receptors differ in output signaling dynamics

To understand how a cell can distinguish signals coming from different chemoattractant receptors, we set out to determine whether the responses differ in the dynamics of activation of major downstream signaling pathways. We focused initially on fMLF (formyl-methionine-leucine-phenylalanine, a model formylated peptide) and LTB4 as model end-target and intermediary chemoattractants, and we used differentiated HL-60 (dHL-60) cells, which are a well-characterized model for human neutrophils. These cells can be differentiated into a neutrophil-like state, and we have previously characterized the broad similarity, as well as specific differences, in gene expression between dHL-60 cells and primary human neutrophils (22).

We measured Cdc42 signaling activity in response to stimulation with a near-saturating dose (6 nM) of LTB4 or fMLF using a previously characterized, genetically encoded FRET sensor (19, 23). For both chemoattractants, the population average Cdc42 response peaked within about 20 seconds, but the response to LTB4 attenuated much more rapidly (Fig. 1B, Movies S1 and S2). After stimulation with LTB4, Cdc42 activity returned to baseline levels about 20–40 seconds after it reached its peak. Conversely, Cdc42 activity remained elevated for more than 2 minutes following fMLF stimulation (Fig. 1B, Movie S2).

To determine whether the difference in signal attenuation arises from inherent properties of the corresponding receptors, FPR1 and LTB4R, or whether it could be explained by receptor sensitivity and the concentrations used, we performed a dose-response analysis. At 0.04 nM, well below the reported dissociation constant of each receptor (24, 25), the Cdc42 responses were similar, with a low amplitude but relatively sustained duration. However, as LTB4 concentrations were increased, it induced stronger but increasingly transient Cdc42 responses (Fig. 1C). In contrast, as fMLF concentrations were increased, response amplitudes also increased, but the responses were sustained (Fig. 1D). For concentrations between 6 and 48 nM, the response patterns remained consistent, with rapid attenuation in response to LTB4 and sustained responses to fMLF (fig. S1, A and B).

Another potential explanation for the difference in dynamics is that stimulation of neutrophils or dHL-60 cells with fMLF promotes the secretion of LTB4 (26). To test whether this secretion affected response duration, we measured responses in the presence of the drug MK-886, which blocks LTB4 production (26, 27). We found that responses to fMLF were unchanged (fig. S1C), indicating that the extended signaling dynamics in response to fMLF are not dependent on autocrine or paracrine LTB4 signaling.

To quantify Cdc42 signaling dynamics more precisely, we measured the time required for the response to fall to its half-maximal level after its peak. As concentrations of LTB4 were increased from 0.4 to 6 nM, the time to half max decreased from ~40 seconds to ~10 seconds (Fig. 1E). For fMLF, the response duration became longer as concentration was increased, and response durations were significantly longer than those for LTB4 (Fig. 1E). Thus, saturating doses of LTB4 do not increase the duration of Cdc42 activation, nor do low doses of fMLF cause transient Cdc42 activity. These results indicate that LTB4R and FPR1 have qualitatively different signaling properties.

Signal attenuation patterns are consistent across signaling outputs, chemoattractants, and in primary human neutrophils

Given that LTB4R and FPR1 have distinct properties for regulating Cdc42, we wondered whether other shared downstream signaling pathways display corresponding differences in signal duration. In neutrophils, chemoattractant stimulation also induces the rapid release of Ca^{2+} from the endoplasmic reticulum (28). The resulting cytosolic Ca^{2+} increase regulates important neutrophil functions such as adhesion and degranulation. To determine whether LTB4 and fMLF stimulation have different effects on the duration of Ca^{2+} signaling, we stained dHL-60 cells with the fluorescent Ca^{2+} indicator dye Fluo-3 and imaged cells before and after the addition of a saturating dose of LTB4 or fMLF. Indeed, we found that LTB4 induced a more transient elevation of cytosolic Ca^{2+} than did fMLF (Fig. 1F), indicating that the chemoattractant-specific kinetics are transmitted to multiple signaling pathways. We note that the dynamics of Ca^{2+} signals at the single-cell level are markedly different from Cdc42 dynamics, including pulsatile and oscillatory behavior (29). However, the consistent trend in signal attenuation at the population level suggests that the difference in signaling output of the receptors probably occurs upstream of both Cdc42 and Ca^{2+}.

Next, we confirmed that differences in signaling properties between LTB4R and FPR1 were present in primary human neutrophils. Although neutrophils are short-lived outside of circulation, the use of a Ca^{2+} indicator dye allows measurement of signaling activity in freshly isolated neutrophils. We also extended our analysis of chemoattractants to include the ChaCha peptide (a C5a analog) that activates the end-target C5aR receptor (30) and the intermediary chemoattractant interleukin-8 (IL-8) that activates CXCR1. Similar to our observations in dHL-60 cells, primary human neutrophils exhibit chemoattractant-specific signaling dynamics. The intermediary chemoattractants LTB4 and IL-8 induced a transient increase in cytosolic Ca^{2+} concentration, whereas fMLF and ChaCha induced a longer lasting Ca^{2+} signal (Fig. 1G). Again, we used the time for the peak response to fall to its half-maximal level as a measure of signal duration. We found no significant difference between chemoattractants of the same class. However, for all comparisons between chemoattractants of different classes, the end-target chemoattractant had a significantly longer signal duration (Fig. 1H). We note that the difference in Ca^{2+} signaling dynamics was smaller in primary neutrophils than it was in dHL-60 cells (Fig. 1, F and G), although the qualitative trend was the same. We conclude that the chemoattractant-specific differences in signaling dynamics in dHL-60 cells are representative of those in primary neutrophils, and that these differences may be a general feature of chemotaxis signaling that distinguishes classes of chemoattractants.

Chemoattractant-specific differences in signaling dynamics are evident in single cells

A limitation of population-level signaling studies is that population averages can mask differences in signaling activity only visible at the single-cell level (31). For example, the dose-dependent increases in amplitudes of Cdc42 activation (Fig. 1, C and D) could be due to increasing single-cell response amplitudes or due to an increase in the fraction of cells responding (with a consistent amplitude for all responding cells). Additionally, the persistence of Cdc42 activity in response to fMLF could be caused by slow attenuation at the single-cell level or by asynchronous pulses of Cdc42 activity that, when averaged, give the appearance of a single, enduring signal. These alternate possible underlying behaviors would have important consequences for understanding signal integration in chemotaxis.

To distinguish between these possibilities, we performed single-cell analysis using data from the Cdc42 kinetics experiments described above. Overall, individual cell responses largely mirrored the population-level Cdc42 dynamics (Fig. 2A). In response to fMLF, single cells maintained persistent activation, rather than asynchronous pulses of activity, and at higher doses of LTB4, signals peaked and attenuated rapidly. However, we also observed apparent increases in the fraction of cells responding, which raised a question of whether responses were graded or “all-or-nothing” at the single cell level (Fig. 2A). Some signaling responses in chemotaxis show signatures of “excitable” behavior, including all-or-nothing responses (32, 33). In contrast, we have previously shown that Cdc42 responds in a graded manner to an optogenetic migration-directing GPCR (34).

To address this question more precisely, we computed histograms of the single-cell Cdc42 response amplitudes. For both chemoattractants, the histograms showed some bimodal character, but there was a clear enrichment of intermediate responses at doses below 1.2 nM (Fig. 2, B and C). The observation that the majority of responding cells in these conditions had sub-maximal amplitudes indicates that the response was indeed graded. The dose-dependent fraction of non-responding cells may arise in large part due to heterogeneity in receptor expression. We have previously measured expression of FPR1 in dHL-60 cells, and found that it can vary widely at the single cell level (22). Furthermore, we found that expression of exogenous LTB4R largely removed the population of nonresponding cells for stimuli of at least 0.6 nM LTB4 (fig. S2, A and B). To analyze the ultrasensitivity of the response, we computed dose response curves considering the 90^{th} percentile response amplitude for each stimulus dose to account for the heterogeneity in receptor expression. We found that the response was moderately ultrasensitive, with hill coefficients between 1 and 2 (Fig. 2D). Analyses using different percentiles gave qualitatively similar results. These results are consistent with the presence of positive feedback in the Cdc42 signaling circuit (34, 35) and the observation of a graded response in which moderate chemoattractant doses cause sub-maximal responses.

We further analyzed the signal attenuation by computing the time for peak responses to fall to their half-maximal levels in single cells. We only included responding cells, and we used an estimate of 100 seconds for cells whose signal had not yet dropped to the half-max value by the end of the time course. As in our population-level analysis, we found that the Cdc42 response attenuated rapidly for higher LTB4 doses, whereas the response to fMLF was sustained across the range of doses (Fig. 2, E and F). The dose-dependent nature of

signal attenuation in response to LTB4 suggests that it is due to rapid negative regulation triggered downstream of LTB4R, acting on a timescale of roughly 10 seconds.

Two phosphorylation sites control rapid signal attenuation for LTB4R

Given the chemoattractant-specific, rapid attenuation of Cdc42 activity, we hypothesized that a negative regulator acts directly on LTB4R, shunting its signaling output. GPCRs contain numerous phosphorylation sites that play important roles in receptor-level regulation. In particular, phosphorylation of serine and threonine residues in the C-terminal tail is associated with ligand-induced receptor-desensitization (36). Two highly-conserved sites in LTB4R are phosphorylated in a ligand-dependent manner – Thr^{308} and Ser^{310} (Fig. 3, A and B) (37). We focused on these residues as candidates for controlling signal attenuation and mutated the sites to alanine, both individually and in combination (Fig. 3B). We generated stable-cell lines exogenously expressing the mutant receptors in the HL-60 Cdc42 FRET-sensor background, reasoning that mutants affecting desensitization should be dominant and should mediate their effects even in the presence of the endogenous WT copies of the gene. As a control, we generated a stable line that exogenously expresses WT LTB4R under the same promoter.

Although the individual T308A and S310A mutations had only small effects on the duration of Cdc42 activation, the double mutant receptors (T308A/S310A) eliminated the rapid signal attenuation, resulting in signaling dynamics similar to those induced by fMLF (Fig. 3, C to E, fig. S3, A to C). The effects were consistent at the population and single cell levels. Cells expressing WT, T308A, or S310A receptors showed dose-dependent decreases in signal duration, but cells expressing T308A/S310A receptors had approximately uniform signal duration for stimulus doses from 0.2 to 12 nM.

Because the p38 and PI3K pathways are implicated in chemoattractant prioritization (12, 14), we tested their contribution to the differences in signaling dynamics using chemical inhibitors. We found that inhibiting PI3K with BKM120 did not affect signal attenuation for either chemoattractant (fig. S4, A and B). For p38, we found that the two inhibitors previously used in studies of neutrophil chemotaxis (8, 14, 38) gave conflicting results depending on both the chemoattractant and the inhibitor used (fig. S4, C and D). Although SB203580 may have caused increased duration of responses to LTB4, BIRB796 had no effect. Considering these results together, it is unlikely that the PI3K and p38 pathways are responsible for the difference in response duration.

To rule out potential confounding effects of receptor overexpression, we confirmed that LTB4R surface expression levels were comparable for all mutant and control lines using flow cytometry (fig. S3D). Therefore, the expression level alone cannot account for the signaling persistence observed in LTB4R-T308A/S310A cells. Our results indicate that both the Thr^{308} and Ser^{310} phosphorylation sites contribute to rapid LTB4R desensitization and that either site alone is sufficient to induce desensitization.

Signal attenuation is not caused by receptor endocytosis

GPCR phosphorylation plays a major role in regulating receptor endocytosis, and phosphorylation can induce desensitization through endocytosis or through endocytosis-

independent mechanisms (36). LTB4R is resistant to endocytosis, which suggests that its desensitization is controlled separately (39, 40). We tested this idea by measuring the effects of the T308A and S310A mutations on ligand-induced receptor internalization by immunocytometry. Consistent with previous studies, we found that only 5–20% of WT LTB4R is internalized in response to 12 nM LTB4 stimulation (Fig. 4, A and B, fig. S5). However, rather than blocking endocytosis, the T308A/S310A double mutation caused increased endocytosis. The effect was almost as strong for the T308A mutation alone, with S310A causing a small synergistic increase in endocytosis but no measurable effect on its own (Fig. 4B, fig. S5). Longer incubation with a higher dose of LTB4 (250 nM) induced higher rates of endocytosis, with about a 50% reduction in surface levels for WT LTB4R, but we found the same qualitative trends for the effects of the mutations (Fig. 4C, fig. S5). Thus, Thr^{308} appears to be critical for limiting LTB4R internalization, with phosphorylation of this residue likely antagonizing internalization. Consistent with this observation, Thr^{308} is separated by only two amino acids from the di-leucine motif in helix 8 that limits LTB4R internalization (Fig. 3B) (40). These results demonstrate that ligand-induced desensitization of LTB4R occurs without large-scale endocytosis and that in fact phosphorylation of Thr^{308} and Ser^{310} may have opposite effects on desensitization and endocytosis.

Mutations affecting LTB4R signal attenuation impair chemoattractant prioritization

Computational studies suggest that differing rates of homologous receptor desensitization, such as what we characterized for LTB4R versus FPR1, could provide a mechanism for chemoattractant prioritization (15). The fast-desensitizing response to LTB4 could drive efficient chemotaxis in the absence of competing signals, but the more sustained output of FPR1 would cause it to dominate in the context of competing gradients. We set out to test this hypothesis by measuring the directionality of dHL-60 cells migrating in competing fMLF and LTB4 gradients.

We developed a simple under agarose chemoattractant prioritization assay in which gradients were established by diffusion from agarose “reservoirs” loaded with either no chemoattractant or a chosen chemoattractant at opposite ends of each well in a 24-well imaging plate (Fig. 5A). Cells migrated under an additional layer of agarose that covered the majority of the well, with chemoattractant gradients formed by diffusion. We then tracked cell movement over time and measured speed and directionality. Using this assay, we found that dHL-60 cells migrated efficiently towards the gradient source for isolated gradients of either fMLF or LTB4 (Fig. 5B, fig. S6A, Movies, S3 and S4). Consistent with prior observations, we found that these cells prioritize fMLF over LTB4 in competing gradients (Fig. 5B, fig. S6A, Movie S5) (41). Similar to cells expressing WT LTB4R, cells expressing the T308A/S310A mutant chemotaxed efficiently to both fMLF and LTB4 in isolated gradients. However, they showed a significant defect in prioritization, migrating with random directionality in the competing gradients (Fig. 5B, fig. S6A, Movie S6).

In our analysis of these experiments, we also noted qualitative differences in the chemotaxis of dHL-60 cells to fMLF compared to LTB4. First, the presence of fMLF seemed to trigger a larger increase in cell speed, although the result was not statistically significant (Fig.

5C). Further experiments will be needed to determine how the chemoattractant conditions differentially affect cell speed.

We also noticed that the movement trajectories of cells migrating in fMLF gradients were straighter, with fewer directional changes, than the trajectories of cells migrating in LTB4 gradients (Fig. 5D, fig. S6B). We quantified the persistence of directionality in migrating cells by measuring the angle between a cell's movement direction at time points separated by defined intervals in time. We found that directional persistence was increased in fMLF gradients but decreased in LTB4 gradients relative to random cell migration in the absence of chemoattractant (Fig. 5E, fig. S6C). We reasoned that this behavior might also result from differences in signaling dynamics, so we measured persistence in cells expressing the T308A/S310A mutant receptor. However, we found that the mutant receptor had no impact on the directional persistence (Fig. 5, D and E, fig. S6, B and C).

Our results indicate that the Thr^{308} and Ser^{310} phosphorylation sites in LTB4R contribute significantly to the ability of neutrophils to prioritize formyl peptides over LTB4 for chemotaxis. However, chemoattractant-specific differences in other aspects of directed movement, such as directional persistence, must arise from different molecular or structural aspects of the receptors.

DISCUSSION

Immune cells guide their migration using a family of GPCRs that activate $G\alpha_i$, but the consequences of activating these receptors are not all the same. Distinctive features of these responses allow neutrophils to efficiently migrate to infection sites by prioritizing signals that emanate from sites of infection and limit their responses to prevent excessive damage (4, 11, 42, 43). However, the receptor elements and molecular mechanisms that determine these differences are not yet resolved, including how receptors detecting "end-target" ligands are prioritized over those detecting inflammatory signals secreted by host cells (4). Our results demonstrate that neutrophil responses to high and low priority chemoattractants differ qualitatively in the duration of signaling outputs. For LTB4R, this difference is determined by two phosphorylation sites in the C-terminal tail of the receptor, Thr^{308} and Ser^{310}, which are necessary for efficient prioritization of formyl peptide chemoattractants over LTB4. Our results, combined with previous mathematical modeling (15), suggest a model in which the rapid desensitization of low priority chemoattractant receptors causes their signals to be overpowered by the longer-lasting signaling output of high priority receptors (Fig. 6).

Receptor desensitization is broadly important for the function of immune cells, including neutrophils. It helps neutrophils self-limit swarming behavior at infection sites and may be important for the reverse migration process that allows neutrophils to return to the vasculature from sites of inflammation. We provide evidence here that receptor desensitization contributes to prioritization of chemoattractants (42, 43). The G-protein coupled receptor kinase (GRK) family plays a fundamental role in this desensitization, but the specific kinases and phosphorylation sites controlling receptor activity are not fully clear. In mice, GRK2 is required for the desensitization that limits LTB4-dependent neutrophil swarming (42), and a study using heterologous expression in COS-7 cells implicated Thr^{308}

as a key residue for GRK6-mediated desensitization of LTB4R (44). Our results indicate that Ser^{310} plays an equally important role for LTB4R desensitization in human immune cells. It remains unclear which kinases regulate these sites, but a combination of GRK2, GRK6, and possibly additional kinases seems likely. In this more complex signaling network, it appears that Thr^{308} and Ser^{310} can each be phosphorylated rapidly, with either modification being sufficient to desensitize the receptor.

The differential homologous desensitization we characterized is likely to work in parallel with other mechanisms to achieve robust prioritization, and the full basis for prioritization may differ between pairs of receptors. There is evidence that downstream crosstalk between the p38 MAP kinase and PI-3-kinase pathways contributes to prioritization (14), although it is not clear how pathways are differentially engaged by the two receptor classes. We did not find evidence that these pathways contribute to the differences in signaling dynamics. Our results showing conflicting effects between different p38 inhibitors are consistent with results for the same two inhibitors in prior studies (38). Further studies, perhaps using specific genetic perturbations, will be necessary to clarify the role of p38 in chemoattractant prioritization. There is also evidence that cross-desensitization contributes in some cases, where lower priority receptors are phosphorylated upon activation of higher priority receptors (16, 45). Even so, our Ca^{2+} signaling results in primary neutrophils using IL-8 and the C5aR ligand ChaCha suggest that the receptor prioritization status may be linked more generally to the rate of desensitization of the corresponding receptors.

Given the marked difference in signaling dynamics, it is interesting that neutrophils chemotax with similar efficiency to both LTB4 and fMLF (Fig. 5B, fig. S6A). A prior study provides a potential explanation, in that chemotaxis to low priority chemoattractants relies largely on temporal sensing, rather than spatial measurement of gradients (9). Temporal sensing typically requires rapid signaling adaptation, allowing cells to sense changes in stimulus levels, rather than absolute levels (46). Because endocytosis-independent desensitization occurs rapidly, this mechanism could be well-suited for a role in temporal sensing by helping to reset downstream signaling on an appropriate timescale. This provides a potential explanation for our result that the phosphorylation sites Thr^{308} and Ser^{310} have opposite effects on desensitization and endocytosis. Non-phosphorylatable mutants limited rapid desensitization but promoted receptor endocytosis. Therefore, phosphorylation of these two residues could quickly tune signaling to promote adaptation for temporal sensing, while keeping the receptors ready for reactivation on the cell surface.

More generally, the behavioral responses triggered by chemoattractant receptors differ in multiple ways. Aside from prioritization status, we found that LTB4 and fMLF drove qualitatively different migration patterns, with fMLF driving more persistent migration with straighter paths and fewer directional turns. The T308A/S310A mutations which blocked the characteristically rapid desensitization of LTB4R did not affect the directional persistence of migration. This finding indicates that chemotactic GPCRs must have multiple sequence or structural differences that underlie chemoattractant-specific features of responses.

MATERIALS AND METHODS

Cloning

Human *LTB4R* cDNA obtained from the Harvard plasmid repository (plasmid #HsCD00003892) was cloned to exogenously express *LTB4R* in HL-60 cell lines. Gibson assembly was used to clone *LTB4R* gene fragments into a lentiviral backbone containing the PGK-1 promoter and the hygromycin resistance gene downstream of an IRES sequence. The T308A, S310A and T308A/S310A mutants were generated by site-directed mutagenesis using 20 cycle PCR reactions with Platinum-SuperFi DNA Polymerase (Invitrogen catalog #12359010). Construction of 3XHA versions of the human *LTB4R* sequence was performed using Gibson assembly. The 3XHA tag sequence was incorporated into primers. One Shot Stbl3 Chemically Competent *E. coli* (Invitrogen catalog #C737303) were transformed to amplify plasmid products. Plasmids were isolated from E. coli using plasmid preparation kits (Sigma) and sequence verified by Sanger sequencing (QuintaraBio). Primers used for cloning are listed in table S1.

Cell culture

HL-60 cells were cultured in RPMI-1640 (Gibco, catalog #72–400-120) media with 9% heat-inactivated fetal bovine serum (FBS) (Sigma-Aldrich, catalog #F4135) and 100 U/ml penicillin-100 mg/ml streptomycin (Gibco, catalog # 15140163). The cell line used for these experiments is also known as PLB-985, which is a subline of HL-60. We have directly verified this genetic identity by SNP analysis (22). These cells were originally obtained as a gift from Dr. Orion Weiner (University of California, San Francisco). Cells were passaged every two to three days and maintained at a culture density between 1.0×10^5 and 2.0×10^6 cells/ml. Cells were differentiated into a neutrophil-like state by culturing at an initial density of 2×10^5 cells/ml in RPMI-1640 with 5% heat-inactivated FBS, 100 mg/ml, 1.3% DMSO, and 2% Nutridoma-CS (Roche, catalog #11363743001) (22). Cells were incubated this way for 6 days before use in experiments, at which point they were referred to as dHL-60 cells. HEK-293T cells (ATCC CRL-11268) were used for lentiviral production. Cells were cultured in high glucose Dulbecco's modified Eagle's medium (Sigma-Aldrich, D5671) that was supplemented with 9% FBS, 1% Glutamax (Gibco, catalog # 35050061), and 100 U/ml penicillin-100 mg/ml streptomycin. All cell lines were maintained in an incubator at 37°C and 5% CO_2. For imaging experiments, a "modified L-15" imaging media (Leibovitz's L-15 media lacking dye, riboflavin, and folic acid) (UC Davis Biological Media Services) was used to minimize media autofluorescence. Cell lines were regularly tested for mycoplasma. No mycoplasma contamination was detected for any cell line used in this work.

Chemoattractants

Multiple chemoattractants were used throughout the experiment, including fMLF (Sigma-Aldrich catalog # 47729), LTB4 (Cayman Chemicals catalog # 20110), IL-8 (ThermoFisher Scientific, catalog # PHC0884), and ChaCha (Anaspec, catalog # AS-65121).

Chemical Inhibitors

Inhibitors were used where specified at the designated concentrations, including MK-866 (Cayman Chemicals catalog # 21753), BIRB-796 (Cayman Chemicals catalog # 10460), NVP-BKM120 (Cayman Chemicals catalog # 11587), and SB203580 (Cayman Chemicals catalog # 13067).

Human primary neutrophil isolation

Ethical approval for the study of neutrophils from adult healthy controls was granted by the Institutional Review Board (IRB) from the University of California, Davis (IORG0000251). Participants gave written, informed consent. Blood was collected by finger prick using a microlet lancing device. Neutrophils were isolated using negative selection with the EasySep Direct Human Neutrophil isolation kit (StemCell, catalog #19666) following the manufacturer's instructions.

Cell-line generation

Stable cell-lines were generated using 2nd generation lentiviral-mediated gene transfer. The packaging vector used was a gift from Dr. Lifeng Xu (pMD.G, University of California, Davis). The envelop vector was a gift from Dr. Peter Lewis (pCMV-dR8.2, University of Wisconsin, Madison). HEK-293T cells were transfected in Opti-MEM (Gibco, catalog # 51985–034) using TransIT-2020 transfection reagent (VWR, catalog # 10767–014). Media was changed to DMEM containing 10% FBS after 12 hours. Supernatant was collected at 24 and 48 hours post media change and filtered (PES 0.45μm; catalog # 25–246). Lentivirus containing supernatant was concentrated 50-fold as described by the manufacturer (Origene, catalog # TR30026), flash frozen in liquid nitrogen and stored at −80°C. HL-60 cells were treated with 50 μl of the concentrated lentivirus and 2 mg/ml Polybrene (Sigma; catalog # H9268–5G). 18 hours later, infected cells were centrifuged (100G; 10 minutes) and resuspended in selection media (supplemented RPMI-1640 with 250 μg/ml Hygromycin). Exogenous, surface expression of receptors was confirmed by flow cytometry.

Uniform chemoattractant stimulation

dHL-60 cells expressing a previously characterized CDC42-FRET sensor (19, 23) were resuspended in warmed modified L-15 media containing 2% FBS at a density of 500,000 cells/ml. To avoid washout, cells were plated on 96-well optical-glass bottomed imaging plates (Cellvis, catalog # P96–1.5H-N) coated with poly-D-lysine ("PDL", Sigma; catalog # P6407). In a sterile tissue-culture hood, 50 μl of 200 mg/ml PDL was added to each well and incubated at room temperature for 30 minutes. After incubation, wells were washed twice with 50 μl sterile DPBS (Life Technologies; catalog # 14190250) and dried thoroughly at 65°C for at least 30 minutes before 100 μl of cells were added (results in ~40–50k cells/well). Before imaging, plated cells were incubated at 37°C for 30 minutes to allow adherence. Time-lapse microscopy was performed using a Nikon Ti-E inverted microscope with a 20x (0.75 NA) Plan Apochromat objective. Images were taken at 5 second intervals. A flash of red light immediately preceding the 4th frame was used to signal the timing for the addition of 100 μl of chemoattractant or media by pipet. To achieve rapid mixing, chemoattractants were added to media at a 1:1 ratio. Images were captured using 2×2

binning. For FRET experiments, Dual Zyla-4.2-USB3 sCMOS cameras were used to capture CFP and YFP channels simultaneously.

Ca^{2+} Assays

dHL-60 or primary neutrophils were centrifuged at 200g for 3 minutes and resuspended in sterile modified L-15 media containing 2% FBS, 2.5 mM probenecid (Life-Technologies: catalog # P36400) and 5 μM Fluo-3 (Life Technologies; catalog # F-14218). Cells were incubated at 37°C for 30 minutes before being centrifuged and resuspended in modified L-15 media containing 2% FBS and 2.5 mM probenecid. Uniform chemoattractant stimulation experiment was performed as described above. Quantification of fluorescent signal from Fluo-3 dye was performed using custom MATLAB scripts. Our image processing workflow included median background subtraction followed by calculation of the mean fluorescence in an image frame. Each independent biological replicate (n) consisted of the mean of three technical replicates. To account for day-to-day variability in Fluo-3 staining, data was first normalized to the mean of the first three frames and then to the mean of the maximum signal for each day.

Flow-cytometry

Flow cytometry data acquired on a BD FACS Canto II flow cytometer (BD Biosciences, Franklin Lakes, NJ) was used to measure receptor internalization and expression of exogenous LTB4R. Flow cytometry data was analyzed using custom MATLAB scripts. Live cells were identified using gates based on FSC and SSC parameters. Surface-expression levels of LTB4R and mutant LTB4R in dHL-60 cells were assessed by immunostaining and flow-cytometry. Cells were harvested, washed with phosphate-buffered saline (PBS) and stained for 30 minutes on ice with a 1:50 dilution of Alexa Fluor-647 conjugated anti-LTB4R antibody (R&D Systems; catalog # FAB099R) in FACS buffer (0.5% bovine serum albumin and 0.05% sodium azide in PBS). After fluorescent labeling, the samples were washed with ice-cold FACS buffer and kept on ice until fluorescence was measured via flow cytometry.

Receptor Internalization Assay

2×10^5 dHL-60 cells in 100 μl were plated on a 96-well Costar assay plate (Corning). 100 μl of either complete medium (as a control) or 2X LTB4 in complete medium were added and mixed well. Cells were incubated at 37°C for either 10 min or 30 min. Samples were then transferred to ice, and centrifugations were performed at 4°C. We performed two washes after incubation using 150 μl FACS buffer (PBS with 5% heat-inactivated FBS and 0.01% sodium azide). The samples were then treated with 25 μl of APC-antiHA antibody diluted 1:75 (~0.07 μg/well, BioLegend catalog # 901523) for 1 hour on ice in the dark. After two washes, the samples were resuspended in 200 μl of FACS buffer and analyzed by flow cytometry. Cells that were not stained were used to determine cellular auto-fluorescence, and cells that did not express an HA-tagged construct were used to set the background signal.

Statistical analysis

Significance values were calculated using tests appropriate for specific experiments. Experiments with comparisons of Cdc42 activity time to half max were made using a non-parametric permutation analysis due to lack of normality and homogeneity of variation in some groups. Permutations were generated using pooled data from all conditions within an experiment. A Monte-Carlo calculation was used to determine the p-value for each comparison. P-values were adjusted using the Bonferroni method to control for the family-wise type I error rate.

For data sets consistent with normal distribution and equal variance assumptions, we used ANOVA followed by Tukey's range test for post-hoc pairwise significance testing which controls for multiple comparisons. This included comparisons of time to half max signal for Ca^{2+} signaling, and comparisons of receptor internalization.

For comparisons of chemotaxis, we used ANOVA followed by Welch's t-test for directed movement, speed, and angular bias measurements. We used the Welch's test for all chemotaxis comparisons as a conservative approach, because the angular bias samples were not consistent with the equal variance assumption. P-values were adjusted by the Bonferroni correction to control for the family-wise type I error rate.

We used Mann-Whitney pairwise testing for comparing directional persistence between samples at each value of delta time. We used this nonparametric approach because the data was not consistent with the normality assumption. Because of the large number of comparisons, we used the Benjamini-Hochberg procedure to account for multiple comparisons by controlling the false discovery rate.

Error bars and shaded error regions represent the standard error of the mean (±SEM) for the indicated number of independent biological replicates (n). To determine whether statistical tests that assume a normal distribution of data could be used, Shapiro-Wilk's test was performed on residuals. To determine if data had homogeneity of variance, Levene's test was used on residuals.

Global and single-cell analysis of FRET images

FRET image pairs were analyzed using custom MATLAB scripts to register the images, subtract background, segment cells, and compute FRET ratios. Image registration was performed as described previously (34) to maximize alignment of cell edges in the two channels throughout the field of view, incorporating xy-translation, rotation, stretch in x and y dimensions, and second order terms to correct for optical aberrations. After registration, an approximation for the camera dark noise (100 intensity units) was subtracted, and a shading correction was applied to correct for unequal illumination and light transmission across the field of view. Background subtraction was performed using the strategy previously described (19). Briefly, an initial objection detection and masking was performed using Otsu's method to determine a threshold and using mask dilation to conservatively exclude cell pixels from the background computation. The background was then computed locally in 64×64 pixel regions as the median intensity of non-object pixels. The background was smoothed to avoid edge artifacts. This background calculation was performed separately for each channel, and

the computed background images were subtracted. To generate cell masks, the two image channels were added together, sharpened using unsharp masking, log transformed, and thresholded. Masks were refined with image opening and the watershed algorithm to reduce noise and separate neighboring cells. Pixels not in the masks were set to NaN (not a number) to exclude them from further analysis. The donor and acceptor images were smoothed with gaussian filter of radius 1.5 pixels to reduce pixel noise. FRET ratio images were computed by diving the acceptor (YFP) image by the donor (CFP) image.

For bulk kinetic analyses, a single FRET ratio for the time point was computed as the sum of all acceptor intensities divided by the sum of all donor intensities, including only pixels in the mask. For single-cell analyses, cells were detected as distinct objects in the mask, and objects with an area below a minimum threshold of 150 pixels or above a maximum threshold of 900 pixels were excluded. The FRET ratio for each cell was computed as the sum of acceptor pixel intensities divided by the sum of donor pixel intensities for pixels in the object. Cells were tracked from frame to frame using a reciprocal nearest neighbor algorithm. Each independent biological replicate (n) consisted of the mean of three technical replicates.

Heatmaps of single cell signaling responses were generated using FRET ratios normalized to the mean of the baseline (3 frames before stimulus). A fraction of the cells are shown in the heatmaps. To make this selection, 167 cells were selected as an even distribution from each biological replicate. For visualization purposes, cells were sorted in descending order of FRET response to stimulus (defined as the mean FRET from frame 4 and later).

To generate histograms of signaling response, the fold change signal was calculated for each cell. We calculated fold change as the max FRET value after stimulus divided by the mean of the baseline. Using MATLAB's 'hist' function, fold change values were sorted into 0.04 sized bins ranging from 0.92 to 2.0 and normalized to a frequency distribution. Each biological replicate (n) was counted as the mean of all values per day.

For the hill plots of the dose-response of Cdc42 signaling amplitudes, we computed the 90^{th} percentile fold-change among cells for each condition for each biological replicate. We used the 90^{th} percentile to estimate response characteristics for cells with high receptor expression, because we have found that heterogeneous receptor expression affects sensitivity to chemoattractant. We have previously found that only approximately 70% of differentiated cells express high levels of FPR1 (22). On a related note, we found that exogenously expressing LTB4R largely eliminated the fraction of cells not responding to LTB4 at intermediate concentrations. Hill curves were fit using least squares regression and the Hill-Langmuir equation.

For violin plots of the Cdc42 response duration in responsive single cells. We defined responsive as meeting a 1.1 fold change above baseline in Cdc42 FRET activity. We computed the time to half-max (t-half) as the time from the max FRET ratio to the first value equal to or less than the value halfway between the max FRET ratio and the baseline FRET ratio. The max FRET ratio was chosen within the first 10 frames after stimulus to ensure the first response to stimulus was captured. If the FRET ratio did not decrease to half

the max or less, time to half max was defined as 100 seconds (the max time possible from the median peak time to the end of image acquisition). The accumulation of cells at 100 seconds indicates cells that had a response duration longer than our imaging period. Violin plots were generated in MATLAB using kernel density estimation with bandwidth set to 2 (seconds).

Under agarose chemotaxis and prioritization assay

To track cell movement in competing chemoattractant gradients, we developed an under agarose imaging assay with chemoattractant containing reservoirs of agarose on opposing sides of a well. 24-well optical-glass bottomed imaging plates (Cellvis, catalog # P24–1.5H-N) were coated with BSA and allowed to dry at 65°C. To prepare chemoattractant reservoirs, 3% low-melting point agarose (Bio Basic, catalog # AB0015) was prepared in modified L-15 media and cooled to 37°C, then mixed at a 1:1 ratio with a 2X concentration of chemoattractant in modified L-15 containing 4% FBS. 100 μl of the chemoattractant/agarose mixture was added to the imaging plate set on a stand holding the plate at a 70° angle above the counter surface. This allowed the agarose to solidify in the corner of the well. After 20 minutes, the plate was rotated and chemoattractant/agarose was added to the opposing side of the well and allowed to solidify for 20 minutes at room temperature. The plate was set flat, and 1.5×10^4 cells stained with 1 μg/ml Hoechst (Life Technologies, catalog # H3570) in 5 μl modified L-15 with 10% FBS were dropped directly in the center of each well. After 5 minutes, 650 μl of 1.5% low melt agarose in modified L-15 containing 2% FBS was slowly added to each well to cover cells and reservoirs. The agarose was allowed to set for 30 minutes at room temperature. The plate was sealed with an aluminum foil cover and incubated for 30 minutes at 37°C. Image acquisition over a 1-hour period at 1 frame/minute began immediately following the warming period.

Tracking and statistics of cell movement

Cell movement was tracked and statistics were computed as described previously (47). Briefly, we used custom MATLAB scripts to identify cells, track them from frame to frame to assemble trajectories, and compute statistics to measure multiple aspects of cell movement. Our image processing workflow included background subtraction, automated cell segmentation, and cell tracking. Cells were tracked from frame to frame by identifying the nearest neighbor in the latter frame for each cell in the prior frame (forward nearest neighbor) and the nearest neighbor in the prior frame for each cell in the latter frame (backward nearest neighbor), and requiring that the two methods agreed. Cell steps from frame to frame were linked to generate cell trajectories.

We used the computed cell trajectories to calculate statistics. For every tracked cell step between adjacent frames, we computed a movement vector to determine distance moved and the angle of movement toward the chemoattractant gradient. An angle of 0° thus represented movement toward the center of the gradient, and an angle of 180° represented movement directly away from the center of the gradient. We applied a minimum distance moved threshold of 13μm (four pixels) for angle measurements to avoid noisy measurements for small movement steps.

We computed a directed movement length as the dot product between the movement vector and the optimal direction unit vector. From the aggregated cell step measurements, we computed mean cell speed as the mean of the movement distances divided by the corresponding time intervals. We computed mean directed movement as the mean of the directed movement distances divided by the corresponding time intervals. We computed angular bias as 90 minus the mean movement angle. Thus, an angular bias of zero corresponds to random direction relative to the gradient, an angular bias of 90 corresponds to maximal directionality toward the center of the gradient, and a negative angular bias corresponds to movement away from the center of the gradient. We computed the cosine of the angle between the direction of movement in the first 30 s and the direction of movement in each subsequent frame-to-frame step. Only cells that moved at least 5 μm in the first 30 s step were included for analysis to capture only moving cells for which an initial direction could be determined accurately. We then computed the mean cosine value for each time point to determine the decay of directional persistence.

Supplementary Material

Refer to Web version on PubMed Central for supplementary material.

Acknowledgments:

We thank the Flow Cytometry Shared Resource at UC Davis and directors Bridget McLaughlin and Jonathan Van Dyke for their support and guidance. We also thank John Albeck, Marie Burns, Mark Huising, and the Collins lab members George Bell, Diana Sernas, Kwabena Badu-Nkansah, and Esther Rincón Gila for critical discussion throughout the project.

Funding:

National Institutes of Health grant DP2HD094656 (SRC)

Sidney Kimmel Foundation Kimmel Scholar Award (SRC)

National Institutes of Health IMSD grant R25GM056765 (BLRG)

Floyd and Mary Schwall Fellowship (BLRG)

Floyd and Mary Schwall Dissertation Year Fellowship (SML)

Lurie Graduate Student Awards (SML)

National Institutes of Health Fellowship F31HL142150 (BLRG)

National Institutes of Health training grant T32GM007377 (SML, SH)

National Institutes of Health P30CA093373

Data and materials availability:

All data needed to evaluate the conclusions in the paper are present in the paper or the Supplementary Materials. Plasmids created for this study are available on Addgene. Due to the large size of the full data set, raw images are not included but are available upon reasonable request. Code used for analysis is also available upon request.

References and Notes:

1. Kolaczkowska E, Kubes P, Neutrophil recruitment and function in health and inflammation. Nat. Rev. Immunol. 13, 159–175 (2013). [PubMed: 23435331]
2. Kunkel EJ, Butcher EC, Chemokines and the tissue-specific migration of lymphocytes. Immunity. 16, 1–4 (2002). [PubMed: 11825560]
3. Segal AW, How neutrophils kill microbes. Annu. Rev. Immunol. 23, 197–223 (2005). [PubMed: 15771570]
4. Lämmermann T, Kastenmüller W, Concepts of GPCR-controlled navigation in the immune system. Immunol. Rev. 289, 205–231 (2019). [PubMed: 30977203]
5. Metzemaekers M, Gouwy M, Proost P, Neutrophil chemoattractant receptors in health and disease: double-edged swords. Cell. Mol. Immunol. 17, 433–450 (2020). [PubMed: 32238918]
6. Ray A, Kolls JK, Neutrophilic Inflammation in Asthma and Association with Disease Severity. Trends Immunol. 38, 942 (2017). [PubMed: 28784414]
7. Huttenlocher A, Smith JA, Neutrophils in pediatric autoimmune disease. Curr. Opin. Rheumatol. 27, 500–4 (2015). [PubMed: 26147757]
8. Boneschansker L, Jorgensen J, Ellett F, Briscoe DM, Irimia D, Convergent and Divergent Migratory Patterns of Human Neutrophils inside Microfluidic Mazes. Sci. Rep. 8, 1887 (2018). [PubMed: 29382882]
9. Petrie Aronin CE, Zhao YM, Yoon JS, Morgan NY, Prüstel T, Germain RN, Meier-Schellersheim M, Migrating Myeloid Cells Sense Temporal Dynamics of Chemoattractant Concentrations. Immunity. 47, 862–874.e3 (2017). [PubMed: 29166587]
10. Foxman EF, Campbell JJ, Butcher EC, Multistep navigation and the combinatorial control of leukocyte chemotaxis. J. Cell Biol. 139, 1349–1360 (1997). [PubMed: 9382879]
11. Campbell JJ, Foxman EF, Butcher EC, Chemoattractant receptor cross talk as a regulatory mechanism in leukocyte adhesion and migration. Eur. J. Immunol. 27, 2571–2578 (1997). [PubMed: 9368612]
12. Heit B, Tavener S, Raharjo E, Kubes P, An intracellular signaling hierarchy determines direction of migration in opposing chemotactic gradients. J. Cell Biol. 159, 91–102 (2002). [PubMed: 12370241]
13. Kim D, Haynes CL, Neutrophil chemotaxis within a competing gradient of chemoattractants. Anal. Chem. 84, 6070–6078 (2012). [PubMed: 22816782]
14. Heit B, Robbins SM, Downey CM, Guan Z, Colarusso P, Miller BJ, Jirik FR, Kubes P, PTEN functions to “prioritize” chemotactic cues and prevent “distraction” in migrating neutrophils. Nat. Immunol. 9, 743–752 (2008). [PubMed: 18536720]
15. Lin F, Butcher EC, Modeling the role of homologous receptor desensitization in cell gradient sensing. J. Immunol. 181, 8335–43 (2008). [PubMed: 19050250]
16. Richardson RM, Ali H, Tomhave ED, Haribabu B, Snyderman R, Cross-desensitization of chemoattractant receptors occurs at multiple levels. Evidence for a role for inhibition of phospholipase C activity. J. Biol. Chem. 270, 27829–27833 (1995). [PubMed: 7499254]
17. Tomhave ED, Richardson RM, Didsbury JR, Menard L, Snyderman R, Ali H, Cross-desensitization of receptors for peptide chemoattractants. Characterization of a new form of leukocyte regulation. J. Immunol. 153, 3267–75 (1994). [PubMed: 8089498]
18. Wang F, The Signaling Mechanisms Underlying Cell Polarity and Chemotaxis. Cold Spring Harb. Perspect. Biol. 1, a002980 (2009). [PubMed: 20066099]
19. Yang HW, Collins SR, Meyer T, Locally excitable Cdc42 signals steer cells during chemotaxis. Nat. Cell Biol. 18, 191–201 (2015). [PubMed: 26689677]
20. Lämmermann T, Renkawitz J, Wu X, Hirsch K, Brakebusch C, Sixt M, Cdc42-dependent leading edge coordination is essential for interstitial dendritic cell migration. Blood. 113, 5703–10 (2009). [PubMed: 19190242]
21. Srinivasan S, Wang F, Glavas S, Ott A, Hofmann F, Aktories K, Kalman D, Bourne HR, Rac and Cdc42 play distinct roles in regulating PI(3,4,5)P3 and polarity during neutrophil chemotaxis. J. Cell Biol. 160, 375–385 (2003). [PubMed: 12551955]

22. Rincón E, Rocha-Gregg BL, Collins SR, A map of gene expression in neutrophil-like cell lines. BMC Genomics. 19, 1–17 (2018). [PubMed: 29291715]
23. Komatsu N, Aoki K, Yamada M, Yukinaga H, Fujita Y, Kamioka Y, Matsuda M, Development of an optimized backbone of FRET biosensors for kinases and GTPases. Mol. Biol. Cell. 22, 4647–4656 (2011). [PubMed: 21976697]
24. Quehenberger O, Prossnitz ER, Cavanagh SL, Cochrane CG, Ye RD, Multiple domains of the N-formyl peptide receptor are required for high-affinity ligand binding. Construction and analysis of chimeric N-formyl peptide receptors. J. Biol. Chem. 268, 18167–18175 (1993). [PubMed: 8349692]
25. Gaudreau R, Beaulieu ME, Chen Z, Le Gouill C, Lavigne P, Staňková J, Rola-Pleszczynski M, Structural Determinants Regulating Expression of the High Affinity Leukotriene B4 Receptor: involvement of dileucine motifs and α-helix VIII. J. Biol. Chem. 279, 10338–10345 (2004). [PubMed: 14688279]
26. Subramanian BC, Majumdar R, Parent CA, The role of the LTB4-BLT1 axis in chemotactic gradient sensing and directed leukocyte migration. Semin. Immunol. 33, 16–29 (2017). [PubMed: 29042024]
27. Gillard J, Ford-Hutchinson AW, Chan C, Charleson S, Denis D, Foster A, Fortin R, Leger S, McFarlane CS, Morton H, Piechuta H, Riendeau D, Rouzer CA, Rokach J, Young R, MacIntyre DE, Peterson L, Bach T, Eiermann G, L-663,536 (MK-886) (3-[1-(4-chlorobenzyl)-3-t-butyl-thio-5-isopropylindol-2-yl]-2,2 - dimethylpropanoic acid), a novel, orally active leukotriene biosynthesis inhibitor. Can. J. Physiol. Pharmacol. 67, 456–464 (1989). [PubMed: 2548691]
28. Bokoch GM, Chemoattractant signaling and leukocyte activation. Blood. 86, 1649–1660 (1995). [PubMed: 7654998]
29. Dupont G, Combettes L, Bird GS, Putney JW, Calcium oscillations. Cold Spring Harb. Perspect. Biol. 3, 1–18 (2011).
30. Servant G, Weiner OD, Herzmark P, Balla T, Sedat JW, Bourne HR, Polarization of chemoattractant receptor signaling during neutrophil chemotaxis. Science. 287, 1037–1040 (2000). [PubMed: 10669415]
31. Albeck JG, Mills GB, Brugge JS, Frequency-modulated pulses of ERK activity transmit quantitative proliferation signals. Mol. Cell. 49, 249–261 (2013). [PubMed: 23219535]
32. Tang M, Wang M, Shi C, Iglesias PA, Devreotes PN, Huang C-H, Evolutionarily conserved coupling of adaptive and excitable networks mediates eukaryotic chemotaxis. Nat. Commun. 5, 5175 (2014). [PubMed: 25346418]
33. Zhan H, Bhattacharya S, Cai H, Iglesias PA, Huang CH, Devreotes PN, An Excitable Ras/PI3K/ERK Signaling Network Controls Migration and Oncogenic Transformation in Epithelial Cells. Dev. Cell. 54, 608–623.e5 (2020). [PubMed: 32877650]
34. Bell GRR, Rincón E, Akdoğan E, Collins SR, Optogenetic control of receptors reveals distinct roles for actin- and Cdc42-dependent negative signals in chemotactic signal processing. Nat. Commun. 12, 1–14 (2021). [PubMed: 33397941]
35. Li Z, Hannigan M, Mo Z, Liu B, Lu W, Wu Y, V Smrcka A, Wu G, Li L, Liu M, Huang C-K, Wu D, Directional sensing requires G beta gamma-mediated PAK1 and PIX alpha-dependent activation of Cdc42. Cell. 114, 215–227 (2003). [PubMed: 12887923]
36. Gurevich VV, Gurevich EV, GPCR Signaling Regulation: The Role of GRKs and Arrestins. Front. Pharmacol. 10, 125 (2019). [PubMed: 30837883]
37. Nakanishi Y, Tan M, Ichiki T, Inoue A, Yoshihara JI, Maekawa N, Takenoshita I, Yanagida K, Yamahira S, Yamaguchi S, Aoki J, Nagamune T, Yokomizo T, Shimizu T, Nakamura M, Stepwise phosphorylation of leukotriene B4 receptor 1 defines cellular responses to leukotriene B4. Sci. Signal. 11, eaao5390 (2018). [PubMed: 30131369]
38. Zhang ER, Liu S, Wu LF, Altschuler SJ, Cobb MH, Chemoattractant concentration-dependent tuning of ERK signaling dynamics in migrating neutrophils. Sci. Signal. 9, ra122 (2016). [PubMed: 27965424]
39. Subramanian BC, Moissoglu K, Parent CA, The LTB4-BLT1 axis regulates the polarized trafficking of chemoattractant GPCRs during neutrophil chemotaxis. J. Cell Sci. 131, jcs217422 (2018). [PubMed: 30158177]

40. Aratake Y, Okuno T, Matsunobu T, Saek K, Takayanagi R, Furuya S, Yokomizo T, Helix 8 of leukotriene B4 receptor 1 inhibits ligand-induced internalization. FASEB J. 26, 4068–4078 (2012). [PubMed: 22707565]

41. Boribong BP, Lenzi MJ, Li L, Jones CN, Super-low dose lipopolysaccharide dysregulates neutrophil migratory decision-making. Front. Immunol. 10, 359 (2019). [PubMed: 30915068]

42. Kienle K, Glaser KM, Eickhoff S, Mihlan M, Knöpper K, Reátegui E, Epple MW, Gunzer M, Baumeister R, Tarrant TK, Germain RN, Irimia D, Kastenmüller W, Lämmermann T, Neutrophils self-limit swarming to contain bacterial growth in vivo. Science. 372, eabe7729 (2021). [PubMed: 34140358]

43. Rocha-Gregg B, Huttenlocher A, Signal integration in forward and reverse neutrophil migration: Fundamentals and emerging mechanisms. Curr. Opin. Cell Biol. 72, 124–130 (2021). [PubMed: 34411839]

44. Gaudreau R, Le Gouill C, Venne M-H, Stankova J, Rola-Pleszczynski M, Threonine 308 within a putative casein kinase 2 site of the cytoplasmic tail of leukotriene B4 receptor (BLT1) is crucial for ligand-induced, G-protein-coupled receptor-specific kinase 6-mediated desensitization. J. Biol. Chem. 277, 31567–31576 (2002). [PubMed: 12077128]

45. Ali H, Richardson RM, Haribabu B, Snyderman R, Chemoattractant receptor cross-desensitization. J. Biol. Chem. 274 (1999), pp. 6027–6030. [PubMed: 10037679]

46. Vladimirov N, Sourjik V, Chemotaxis: how bacteria use memory. Biol. Chem. 390, 1097–104 (2009). [PubMed: 19747082]

47. Collins SR, Yang HW, Bonger KM, Guignet EG, Wandless TJ, Meyer T, Using light to shape chemical gradients for parallel and automated analysis of chemotaxis. Mol. Syst. Biol. 11, 804 (2015). [PubMed: 25908733]

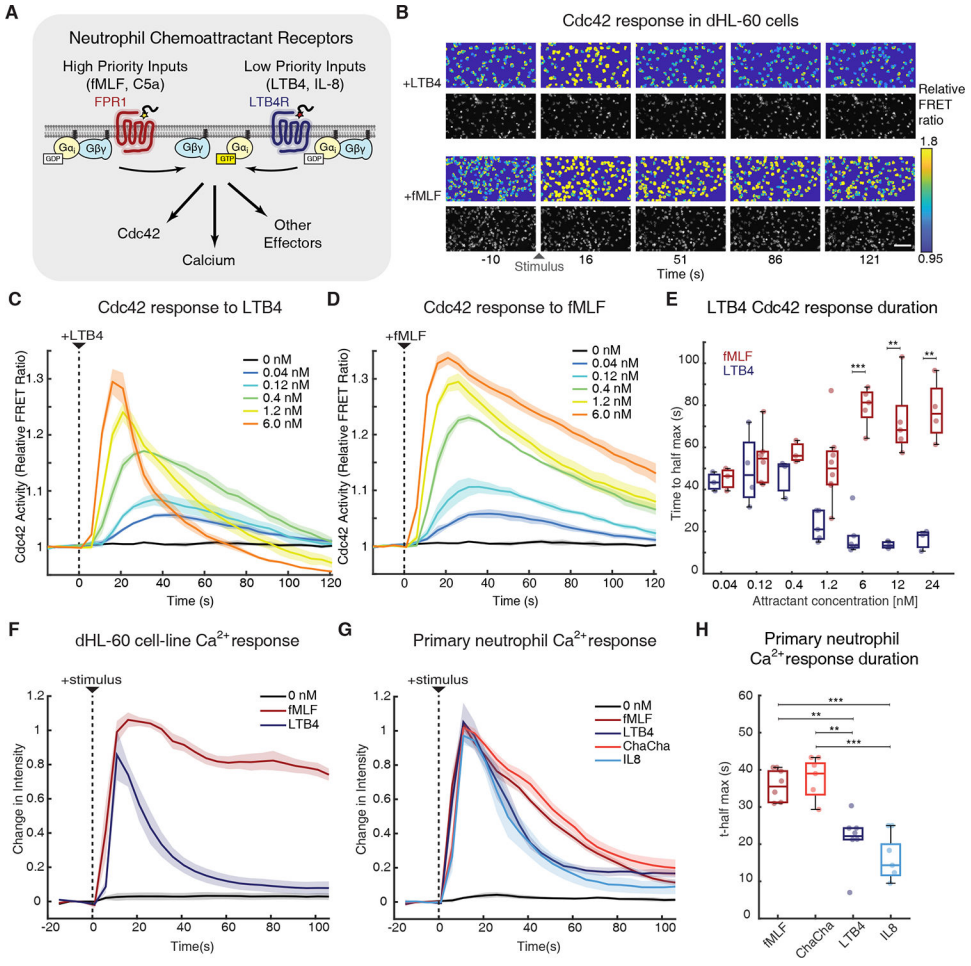

Fig. 1. Low priority chemoattractant receptors have faster signal attenuation than high priority receptors.

(**A**) High and low priority receptor activation leads to a common downstream signaling cascade driven by effectors of $G\alpha_i$ and $G\beta\gamma$ subunits. (**B**) Neutrophil-like differentiated HL-60 (dHL-60) cells expressing a Cdc42 FRET sensor were imaged at 5 second intervals before and after stimulation with 6 nM LTB4 or fMLF stimulus. Representative images show pseudo-colored relative FRET ratio above and grayscale of fluorescent intensity below. Scale bar, 100 μm. (**C**, **D**) Quantification of Cdc42 dynamics in response to stimulation with different concentrations of LTB4 or fMLF (n=3 biological replicates for each condition). (**E**) Boxplot showing the Cdc42 response durations calculated as the time from peak signal to half-maximal value. Dots indicate independent biological replicates. P-values for comparisons between fMLF and LTB4 samples at each concentration were calculated using a permutation approach and adjusted using the Bonferroni correction (7 comparisons). (**F**, **G**) Cytosolic Ca^{2+} dynamics in response to stimulation with the indicated chemoattractants were measured by imaging dHL-60 or primary human neutrophils stained with Fluo-3 dye at 5 second intervals. Cells were treated with a saturating dose of “end-target” chemoattractants fMLF (24 nM) or the C5aR agonist ChaCha peptide (1 μM), or “intermediary” chemoattractants LTB4 or IL-8 (24 nM). Data was normalized according to the pre-stimulus baseline and the mean maximum signal for all conditions to account for

staining variability. (**H**) Boxplot of the times from peak signal to half-maximal value for primary neutrophil Ca^{2+} responses. P-values were calculated using Tukey's range test. Dots indicate biological replicate measurements. Curves and shaded error regions represent the mean ± SEM over biological replicate measurements. Boxes in the boxplots indicate the 25^{th} and 75^{th} percentiles, with the center bar indicating the median, and whiskers indicating the range of the data aside from automatically determined outliers. No symbol for p-value > 0.05, * for p-value < 0.05, ** for p-value < 0.01, and *** for p-value < 0.005 for figure panels where statistical calculations are indicated.

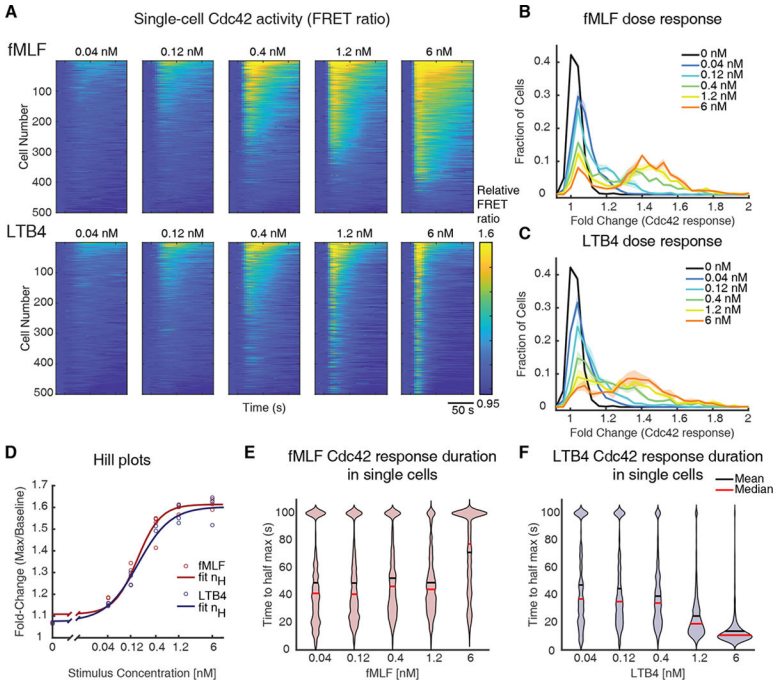

Fig. 2. Single-cell kinetics are consistent with bulk analysis and reveal a graded response.

Data presented in Fig. 2 are single cell information extracted from the experiments shown in Fig. 1C, D. (**A**) Heat maps displaying Cdc42 FRET ratios over time on a single cell basis. For each concentration, 500 cells were selected as an even distribution of all cells analyzed. Data shown is arranged in descending order from top to bottom by the mean of the FRET ratio after stimulus. (**B**, **C**) Histograms displaying the frequency distributions of the single cell fold-change in Cdc42 FRET ratio, comparing the maximum after stimulus to the baseline before stimulus. (**D**) Hill plots of Cdc42 response to chemoattractants. Dots indicate independent biological replicates and the lines indicate the Hill-fit. Hill coefficient (n_H) for fMLF = 1.80 ± 0.25 and for LTB4 = 1.28 ± 0.04. (**E**, **F**) Violin plots showing the distribution of Cdc42 response duration in response to fMLF (E) and LTB4 (F) among single cells.

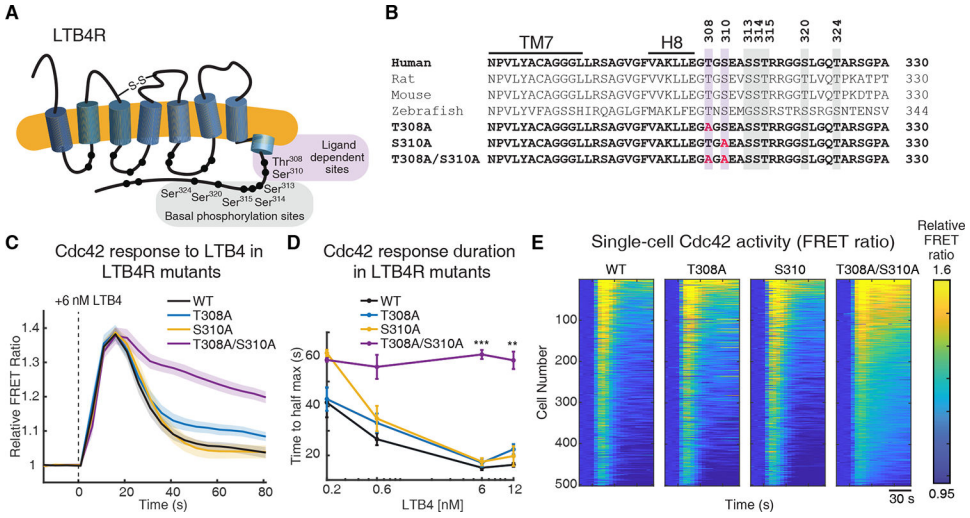

Fig. 3. Rapid signal attenuation in response to LTB4 depends on the phosphorylation sites Thr^{308} and Ser^{310} in the LTB4R receptor.

(**A**) Schematic showing the LTB4R GPCR and phosphorylation sites in the C-terminal tail of the receptor. Phosphorylation sites highlighted in purple are ligand-dependent, and those in grey are basally phosphorylated. (**B**) Amino acid sequence alignment of a section of LTB4R showing conservation across multiple metazoan species. Phosphorylation sites are highlighted using the color scheme in (A). Phosphorylation sites substituted with alanine residues by site directed mutagenesis are shown in red. TM7= trans-membrane helix 7, H8 = helix 8. (**C**) Plots showing the relative Cdc42 FRET ratio of dHL-60 cells expressing versions of the LTB4 receptor under the same promoter. Images were acquired at 5 second intervals before and after 6 nM LTB4 stimulus. Curves and shaded error regions represent the mean ± SEM over at least five biological replicate measurements per group. (**D**) Signal duration of the data in (C) was measured as time to half maximum as a dose response curve comparing mutant versions of the LTB4 receptor. P-values were calculated for comparisons between each pair of receptors within each concentration using a permutation approach with the Bonferroni correction (12 comparisons). (**E**) Single cell data was extracted from the experiment shown in (C) and (D). Single cell changes in Cdc42 activity are shown on heat maps, which compare different versions of the LTB4 receptor stimulated with 6 nM LTB4. 500 cells shown were selected as an even distribution from all cells.

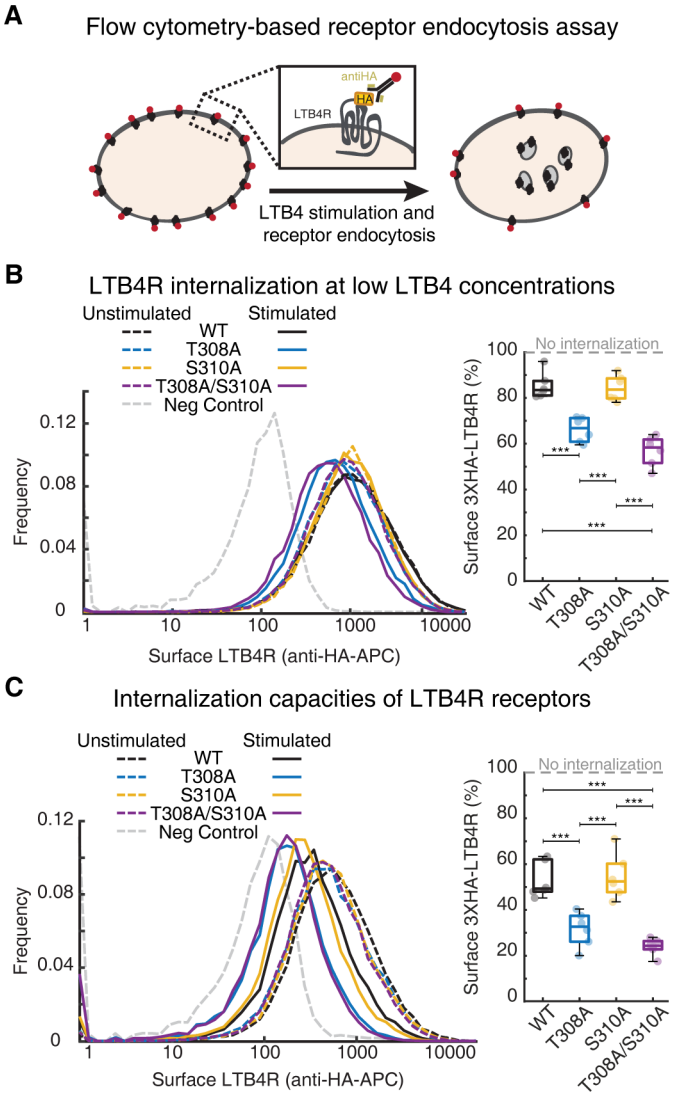

Fig. 4. The phosphorylation sites Thr^{308} and Ser^{310} limit LTB4 receptor endocytosis.

(**A**) A schematic depicting detection of LTB4R endocytosis measured by loss of fluorescent signal. Versions of LTB4R tagged with 3xHA (hemagglutinin-tag) were expressed in dHL-60 cells for quantification by immunocytometry for HA. Comparison of cells stained without compared to with LTB4 stimulation was used to determine the percentage of receptor remaining on the surface. Allophycocyanin (APC) signal (LTB4R on the cell surface) was measured by flow cytometry. (**B**) Representative histograms showing LTB4R cell surface levels. Cells were either unstimulated or stimulated with 12 nM LTB4 for 10 minutes prior to immunostaining for HA (left). Boxplot (right) quantifying receptor internalization of LTB4R. 100% is defined as the surface LTB4R level in unstimulated cells and indicates no internalization of the receptor. Data represent 5 independent biological replicates per group. (**C**) Data showing experiments as performed in (B) but with cells stimulated with 250 nM LTB4 for 30 minutes to obtain maximal internalization of the receptors. Data represent 5 independent biological replicates per group. P-values were calculated using Tukey's range test.

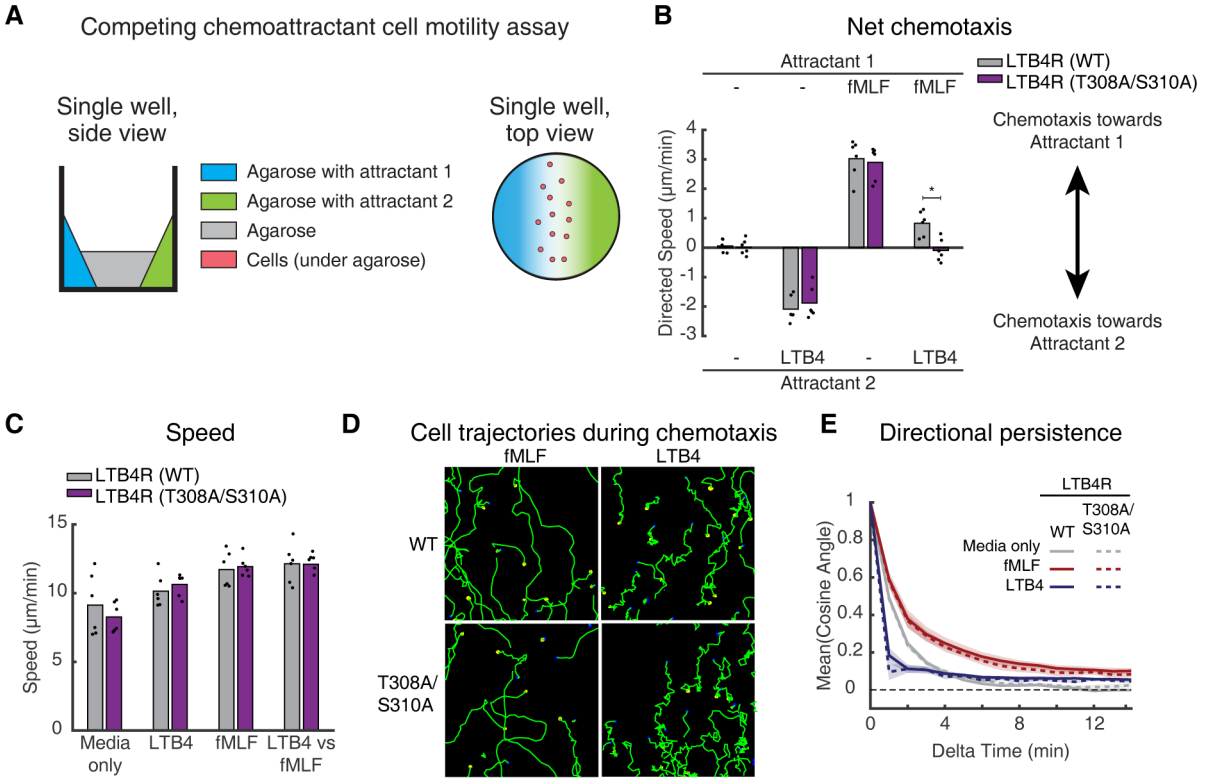

Fig. 5. The phosphorylation sites Thr^{308} and Ser^{310} in LTB4R are necessary for chemoattractant prioritization.

(**A**) A diagram displaying the layout of a microscopy-based competing chemoattractant chemotaxis assay performed in a 24-well plate format. Cells move across the imaging plate surface under 1.5% agarose. Diffusion-based gradients were created by adding chemoattractant to “reservoirs” on one or both sides of the well and cell movement can be tracked over time by imaging (**B**) Chemotaxis of dHL-60 cells expressing LTB4R wild-type (WT) or LTB4R (T308A/S310A) was compared using the assay described in (A). Cells were stained with Hoechst and images were acquired for 60 minutes at a rate of 1 frame/minute. Net chemotaxis was defined as directed speed of cells toward fMLF (positive) or LTB4 (negative) and was measured as the rate of movement of the cell in the direction of the gradient source. Dots indicate independent biological replicates (n = 6 per group). P-values for comparisons between WT and T308A/S310A were calculated using Welch’s t-test and corrected with the Bonferroni method (4 comparisons). (**C**) Bar graph showing the average speed of cells in (B). (**D**) Images showing representative traces (green) of cell movement over 60 minutes. The initial image (blue) was merged with the final image (yellow) to show the starting and ending locations of the cells. (**E**) A plot showing the directional persistence of cell movement, defined as the mean cosine of the angle between a migrating cell’s movement direction at two different time points was measured as a function of the difference in time between the two measurements. Cells migrating in a straight line would have a mean cosine angle of 1. Curves and shaded error regions represent the means ± SEM for 6 biological replicates per group.

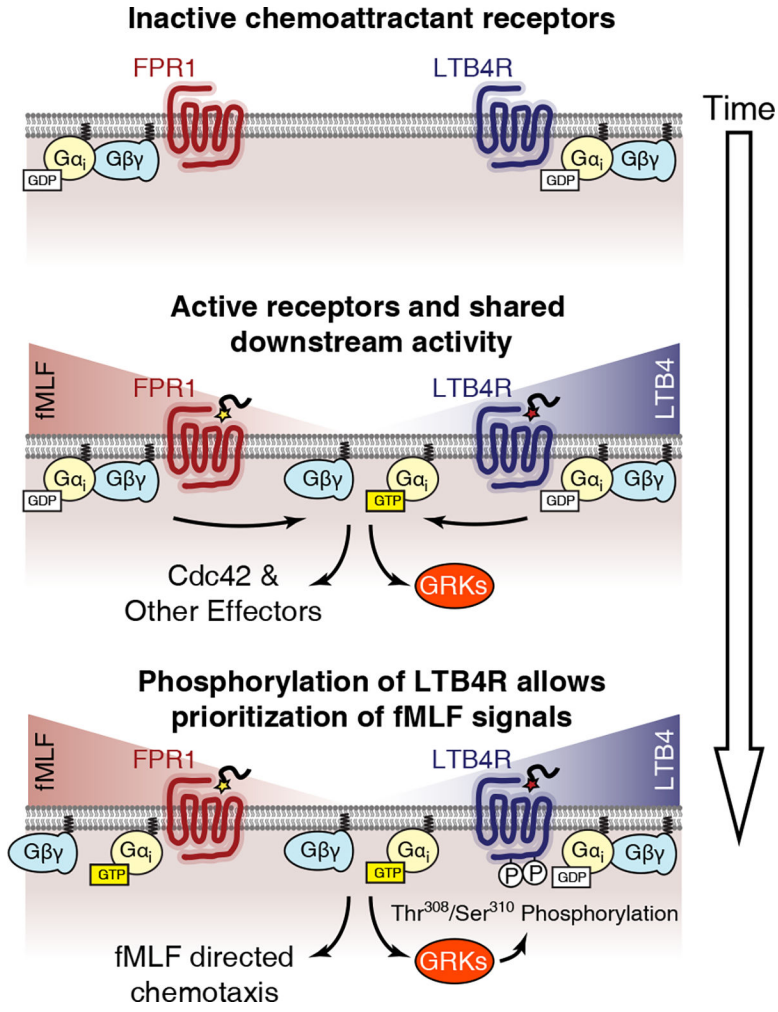

Fig. 6. Shared signaling networks between chemoattractant receptors allow for prioritization of fMLF over LTB4 signals.

A diagram displaying our model of signal transduction in response to multiple chemoattractant stimuli. In a resting state (top), receptors are inactive with guanosine diphosphate (GDP) bound G-proteins. Exposure to chemoattractant gradients (middle) activates the receptors, leading to dissociation of G-proteins in their guanosine triphosphate (GTP)-bound state and activation of downstream signaling pathways. Following stimulus, GRKs rapidly phosphorylate LTB4R (bottom), thereby switching the receptor off. The rapid desensitization of LTB4R allows the neutrophil to prioritize fMLF signals, and the cell will move in an fMLF-directed manner.